Electronic States of Al_3P_2, Al_2P_3, and Their Ions

K. Balasubramanian*,† and Ping Yi Feng‡

Department of Applied Science, University of California Davis, P.O. Box 808, L-794, Livermore, California 94550, Chemistry & Material Science Directorate, Lawrence Livermore National Laboratory, University of California P.O. Box 808, L-268, Livermore, California 94550, Glenn T. Seaborg Center, Lawrence Berkeley National Laboratory, Berkeley, California 94720, and State Key Laboratory of Functional Materials for Informatics, Shanghai Institute of Metallurgy, Academia Sinica, Shanghai 200050, China

Received: July 17, 2001; In Final Form: September 27, 2001

Complete active-space self-consistent field (CASSCF) method followed by multireference singles + doubles configuration interaction (MRSDCI) calculations that included up to 4 million configurations were carried out on the electronic states of Al_3P_2, Al_2P_3 and their anions and cations. Our computed results explain the recently reported anion photoelectron spectra of $Al_2P_3^-$ and $Al_3P_2^-$ by Neumark and co-workers.[1] We find that both the $Al_2P_3^-$ and Al_2P_3 species have D_{3h} undistorted trigonal bipyramidal structures consistent with the sharp and intense ground-state peak in the observed spectra. But the neutral Al_3P_2 cluster was found to be Jahn−Teller distorted in contrast to the $Al_3P_2^-$ anion, which has a D_{3h} undistorted trigonal bipyramidal structure, consistent with the observed extended vibrational progression of the X state of the spectra. Our computed electron affinities agree well with the onsets of the observed X peaks in both spectra. We assign the partially resolved vibrational structure in the observed spectra to the totally symmetric stretch mode than to symmetry lowering of Al_2P_3, which is found to be in a $^2A_2''$ (D_{3h}) state and cannot undergo Jahn−Teller distortion. Seven electronic states of Al_3P_2 are computed, among which the $^2A_1$(C_{2v}) state is the ground state with a distorted trigonal bipyramid structure. The distorted$^2A_1$ and $^2B_1$ (C_{2v}) states are identified as Jahn−Teller components of the undistorted $^2E'$ and $^2E''$ (D_{3h}) states, respectively. Properties of four electronic states of Al_2P_3, $Al_3P_2^+$, and $Al_2P_3^+$ are also reported. The ground states of both $Al_3P_2^+$ and $Al_2P_3^+$ are undistorted $^3A_2'$ and $^1A_1'$, respectively (D_{3h} symmetry). The atomization energy, adiabatic ionization potentials, dipole moments, and other properties for the electronic states of Al_3P_2 and Al_2P_3 are calculated and discussed. Comparisons are made with the Ga and In analogues of these species.

I. Introduction

The present theoretical study on the low-lying electronic states of the Al_3P_2 and Al_2P_3 clusters and their anions was motivated by a recent and the first experimental work by Gomez et al.[1] on the anion photoelectron spectroscopy of aluminum phosphide clusters including mixed pentamers. A striking contrast between the observed spectra of $Al_2P_3^-$ and $Al_3P_2^-$ is that the former exhibits a sharp single band corresponding to the neutral ground state of Al_2P_3, whereas the latter exhibits an extended progression in the ground state followed by a few other peaks attributable to the excited states of Al_3P_2[1]. In fact, an excited state of Al_3P_2 exhibits a more intense peak compared to the X ground state. The $Al_2P_3^-$ spectrum exhibits partially resolved vibrational structure (separation of 465 cm^{-1}), and it is not clear if this is due to symmetry lowering of the ground state of Al_2P_3 or due to Franck−Condon activity from the lower frequency Al−Al stretch. Gomez et al. have reported the adiabatic electron affinities of these species on the basis of the observed onsets for the X peaks. It is interesting that both Al_3P_2 and Al_2P_3 have similar electron affinities although the observed spectra are different suggesting geometry differences and excited states with different energies for the two clusters.

The group 13−15 clusters have been the topic of many studies[2−38] in recent years not only due to their intrinsic merit but also due to their technological importance, as group 13−15 materials find applications in high speed and high luminosity semiconductor devices and light-emitting diodes. Smaller clusters are intriguing in that they do not evolve smoothly as a function of their sizes to the bulk, as they exhibit dramatic variations in their properties, spectra and relative abundance.

There have been many experimental studies[2−24] on group 13−15 clusters after an inspiring experimental work by Smalley and co-workers[9] on Ga_xAs_y. This was the first work that demonstrated that smaller clusters of Ga_xAs_y are substantially different from larger ones in that smaller clusters exhibit remarkable deviation from the anticipated binomial distribution while larger ones followed the binomial distribution. It was also predicted by one of the authors[26] that clusters of Ga_xAs_y would exhibit isomers. Spectroscopy of 13−15 clusters has been made possible with the advent of the supersonic beam method in which a source material of the group 13−15 compound is laser-evaporated and passed through a supersonic nozzle, which results in cooling and copious amounts of clusters of different compositions.[6] A variety of spectroscopic techniques have been invoked to study these clusters with the intent of probing the low-lying electronic states of these clusters.

* To whom correspondence should be addressed. E-mail: kbala@ucdavis.edu.

† University of California Davis, Lawrence Livermore National Laboratory, and Lawrence Berkeley National Laboratory.

‡ Shanghai Institute of Metallurgy.

10.1021/jp012764m CCC: $20.00
Published on Web 11/20/2001

Neumark and co-workers[1−7,13−15] have obtained the anion photoelectron spectra and zero-electron kinetic energy (ZEKE) photodetachment spectra of 13−15 anions such as $Ga_xP_y^-$, $In_xP_y^-$, and $Ga_xAs_y^-$, $Al_xP_y^-$ clusters. In this method, they obtain the photoelectron spectra starting with the size-selected anions by photoexciting the anion to probe the ground and excited states of the neutral species. The technique yields both electronic and vibrational information on the neutral species, while the ZEKE spectra have considerably higher resolution. Experimental studies of other 13−15 clusters such as Al_xAs_y, etc., are in progress.[3] These experiments have yielded not only electron affinities but also the term values for the low-lying electronic states of neutral clusters through the measured vertical detachment energies of various peaks. In addition, for certain clusters, the vibrational frequencies of the neutral and anionic clusters have been reported if the spectra had sufficient resolution.

The aluminum phosphide clusters are particularly attractive, as they have higher vibrational frequencies (due to lower masses) and, thus, as noted by Gomez et al.,[1] could result in vibrational progressions in the spectra compared to heavier clusters. To the best of our knowledge, Gomez et al.[1] were the first to report the spectra of aluminum phosphide clusters including Al_2P_3 and Al_3P_2. Taylor et al.[15] have recently reported high-resolution vibrationally resolved anion photoelectron spectra of GaX_2^-, Ga_2X^-, $Ga_2X_2^-$, and $Ga_2X_3^-$ anions for X = P and As.

Weltner and co-workers[11,12] have employed matrix-isolation techniques in combination with the ESR or far-IR spectroscopic methods to study a few 13−15 clusters. These techniques have yielded the ground-state geometries and spin multiplicities of some of these species from the observed hyperfine patterns. These authors[11] have obtained the far-infrared spectra of Ga/P, Ga/As, and Ga/Sb clusters in rare-gas matrixes at 4 K. Van Zee et al.[12] have obtained the hyperfine interaction and structure of Ga_2As_3 using the matrix-isolated ESR spectra of these species. The hyperfine pattern exhibited a doublet ground state with a trigonal bipyramid structure (tbp) in a probable ground state of $^2A_2''$.

Duncan and co-workers[19−22] have employed photoionization and photodissociation techniques to extract important information on the photofragmentation patterns and spectroscopic properties on the excited states of the cations of such clusters. At present, these techniques have been used to study mixed heavier cations such as $In_xSb_y^+$.

Theoretical studies on the electronic states of larger 13−15 clusters have often been restricted to the ground states, although smaller ones up to five atoms have been investigated for the excited states.[25−41] As demonstrated by our past work,[30−32,39−41] investigation of the excited states of these species is quite challenging. We have utilized ab initio CASSCF and MRSDCI techniques to compute the properties of the excited electronic states. Although we and others have studied other five-atom clusters such as Ga_3As_2, the current theoretical study is the first of its kind to focus on the ground state and several low-lying excited electronic states of the mixed pentamers containing Al and P. We have studied before other smaller Al_xP_y clusters[39] both in the ground and excited states, and Raghavachari and co-workers[33] have studied the ground states of $(AlP)_n$ clusters using the MP4 and QCISD(T) methods. There have been DFT studies on $(AlP)_n$ clusters,[35] and smaller Al_xP_y clusters[34] have been studied by a number of other techniques. The diatomics of 13−15 elements have also been studied, and potential energy curves of many excited electronic states have been obtained.[27,38] In the current study, we compute the low-lying electronic states of Al_3P_2 and Al_2P_3 and their positive and negative ions using high-level relativistic ab initio CASSCF and MRSDCI techniques that included up to 4 million configurations. We consider full geometry optimization for both ground and excited states, including the possibility of Jahn−Teller distortions.

II. Method of Computations

We have employed state-of-the-art computational techniques to study the electronic states of Al_2P_3, Al_3P_2, and their ions (both cations and anions). The theoretical techniques included a complete active space self-consistent field (CASSCF) technique followed by multireference singles + doubles CI (MRSDCI) computations. All of the computations were made using relativistic effective core potentials (RECPs) that retained the outer $3s^23p^1$and $3s^23p^3$ shells of Al and P, respectively, in the valence space replacing rest of the electrons by RECPs. The RECPs, together with valence Gaussian basis sets, were taken from the work of Pacios et al.[42] These basis sets were augmented with a set of 3d polarization functions with exponent of 0.3084 for Al and two sets of 3d functions ($\alpha_1 = 1.20$, $\alpha_2 = 0.3$) for P.

In the CASSCF technique, energetically low-lying 3s orbitals of the Al and P atoms were kept inactive in the sense that excitations were not allowed, but they were allowed to relax as a function of geometry. All of the remaining orbitals were included in the active space, and all possible excitations among these orbitals were allowed to generate a full CI space for the CASSCF. This choice yielded an active space comprising three a_1, two b_2, three b_1, and two a_2 orbitals for Al_3P_2, Al_2P_3, and their ions. Nine active electrons for Al_3P_2 (or eight electrons for $Al_3P_2^+$ and 10 electrons for $Al_3P_2^-$) and 11 active electrons for Al_2P_3(or 10 electrons for $Al_2P_3^+$ and 12 for $Al_2P_3^-$) were distributed among all possible orbitals at the CASSCF stage. Subsequently, multireference singles + doubles configuration interaction (MRSDCI) calculations that included all configurations in the CASSCF with absolute values of coefficients ≥ 0.07 were carried out. This generated a large configuration space that included up to 4 million configurations. After the MRSDCI, multireference Davidson correction to the MRSDCI energy was invoked, and the resulting computed energy separations were labeled as MRSDCI + Q.

Analogous to the previous study[31] on Ga_3P_2 and Ga_2P_3, we started with geometry optimization for the low-lying electronic states of Al_3P_2 and Al_2P_3, using a quasi-Newton−Raphson procedure within the CASSCF level of theory. For this purpose, the GAMESS[43] package of molecular computational codes was employed to generate the optimized geometry in the C_{2v} symmetry. Two electronic states, namely, $^2A_1$ and $^2B_1$ of Al_3P_2 (or $^2A_2$ and $^2A_1$ for Al_2P_3), are found to be formed from $^2E'$ and $^2E''$ (D_{3h}). Since the $^2E'$ and $^2E''$ states are in doubly degenerate irreducible representations, they undergo Jahn−Teller distortions through E⊗e coupling. The geometries of all possible low-lying doublet and quartet electronic states for Al_3P_2 and the low-lying doublet states of Al_2P_3 in the D_{3h} symmetry were searched and optimized.

The knowledge of the electronic states of the $Al_3P_2^+$ and $Al_2P_3^+$ positive ions would be useful for experimental photoionization spectroscopic studies of the neutral species. Furthermore, it is critical to obtain the ground-state information on the anions so that the anion photoelectron spectra can be interpreted. For example, Gomez et al.[1] have recently measured the electron affinities of the anions of the aluminum phosphide Al_xP_y (x, y = 1−4) clusters. Consequently, in the current study, we have pursued theoretical calculations on the electronic states of the $Al_3P_2^+$, $Al_2P_3^+$, $Al_3P_2^-$, and $Al_2P_3^-$. The atomization energies

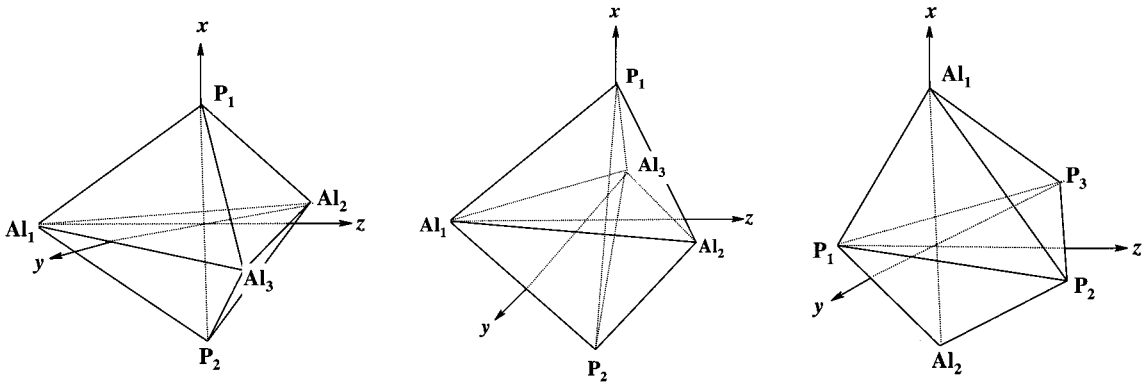

Figure 1. Geometries of distorted and undistorted mixed pentamers.

TABLE 1: Geometries and Energy Separations for the Electronic States of Al_3P_2 and Al_2P_3 in C_{2v} Structure

		state (C_{2v})	
state		$^2A_1$	$^2B_1$
Al_3P_2	$Al_2-Al_1-Al_3$ (deg)	69.5	70.9
	$P_1-Al_1-P_2$ (deg)	64.8	48.0
	$P_1-Al_2-P_2$ (deg)	57.3	50.7
	Al_1-Al_2 (Å)	3.529	3.801
	Al_2-Al_3 (Å)	4.023	4.409
	Al_1-P_1 (Å)	2.279	2.680
	Al_2-P_1 (Å)	2.547	2.543
	P_1-P_2 (Å)	2.443	2.178
	dipole moment (D)	−2.69	−1.34
	E (CASSCF) (eV)	0.00	0.48
	E (MRSDCI) (eV)	0.00	0.60
	E (MRSDCI + Q) (eV)	0.00	0.51
		$^2A_2$	$^2A_1$
Al_2P_3	$P_2-P_1-P_3$ (deg)	53.8	58.0
	$Al_1-P_1-Al_2$ (deg)	141.9	115.8
	$Al_1-P_2-Al_2$ (deg)	111.0	114.1
	P_1-P_2 (Å)	2.315	2.302
	P_2-P_3 (Å)	2.093	2.232
	P_1-Al_1 (Å)	2.506	2.425
	P_2-Al_1 (Å)	2.874	2.448
	Al_1-Al_2 (Å)	4.736	4.110
	dipole moment (D)	−0.99	−0.26
	E (CASSCF) (eV)	0.19	2.10
	E (MRSDCI) (eV)	0.48	1.96
	E (MRSDCI + Q) (eV)	0.64	1.93

to dissociate the Al_3P_2 and Al_2P_3 clusters into aluminum (^2P) and phosphorus (^4S) atoms were computed as supermolecular calculations.

The CASSCF/MRSDCI calculations were made using one of the authors[44,46] modified version of ALCHEMY II codes[45] to include relativistic ECPs (RECPs).

III. Results and Discussions

A. Electronic States of Al_3P_2. Table 1 lists the optimized geometries and energy separations together with dipole moments for the distorted $^2A_1$ and $^2B_1(C_{2v})$ states of Al_3P_2. The equilibrium geometries and energy separations for all undistorted doublet and quartet electronic states of Al_3P_2 in the trigonal bipyramid structure (D_{3h}) are shown in Table 2. Table 3 shows our computed vibrational frequencies of the ground states of the various species. The actual locations of the atoms for both distorted and undistorted Al_3P_2 are shown in Figure 1. As seen from Table 2, the first two undistorted low-lying electronic states of $Al_3P_2(D_{3h})$ are $^2E'$ and $^2E''$ and would thus undergo the Jahn−Teller distortion. So the distorted $^2A_1$ and $^2B_1(C_{2v})$ states of Al_3P_2 in Table 1 are the Jahn−Teller components of the $^2E'$ and $^2E''$ (D_{3h}), respectively. The $^2A_1(C_{2v})$ state is 0.33 and 0.23 eV lower than its corresponding state $^2E'(D_{3h})$ due to Jahn−Teller stabilization, while the $^2B_1(C_{2v})$ state is 0.17 and 0.04 eV lower than the $^2E''(D_{3h})$ state at the CASSCF and MRSDCI levels of theory, respectively. The $^2A_1$ state prevails as the ground state of Al_3P_2 at all levels of theory, and the $^2B_1$ state is 0.48 and 0.60 eV above the ground state at the CASSCF and MRSDCI levels, respectively. As mentioned before, the $^2A_1$ and $^2B_1$ states (C_{2v}) could be envisaged as derivatives of the $^2E'$ and $^2E''$(D_{3h}) states arising from Jahn−Teller distortion. This can be shown by their geometry parameters, which present an interesting relationship between various states. As can be seen from Table 1, there are two contracted Al_1-Al_2 and Al_1-Al_3 (3.529 Å) bonds together with an elongated Al_2-Al_3 (4.023 Å) bond in the $^2A_1(C_{2v})$ state. Likewise, the P−P bond lengths in the $^2A_1(C_{2v})$ and $^2E'(D_{3h})$ states of Al_3P_2 are 2.443 and 2.516 Å, respectively. These features suggest that the Jahn−Teller effect primarily moves the three Al atoms from their ideal D_{3h} equilateral triangular locations in the Al_3P_2 cluster and brings the two axial P atoms closer forming a more stable distorted structure (C_{2v}). The P−P bond length of the diatomic P_2 is 1.893 Å in its $^1\Sigma_g^+$ ground state[51], while the P−P bond length in the $^2A_1(C_{2v})$ state of Al_3P_2 is 2.44 Å. On the other hand, the Al−Al bond lengths in the $^2A_1$ ground state of Al_3 are around 2.54 Å[47] and are much shorter compared to the Al−Al bond lengths (3.62−4.03 Å) in Al_3P_2. Evidently, the bonds among the three Al atoms in Al_3P_2 are dramatically weakened by the Al−P bonding and the interaction between the two P atoms. All the quartet states in the undistorted D_{3h} structure were also computed. These states, namely, $^4A_2''$, $^4E''$, and $^4E'$, are well above the ground state.

B. Electronic States of $Al_3P_2^+$, $Al_3P_2^-$, Ionization Energy, Electron Affinity, and Binding Energies. Four low-lying electronic states of $Al_3P_2^+(D_{3h})$ were computed, and their energy separations are shown in Table 2. We kept the geometry of the positive ion fixed at the neutral $^2E'$ geometry because we do not expect the geometry relaxation to make a significant impact on the computed ionization energy. The excited electronic states of $Al_3P_2^+$ can be visualized as arising from the removal of an electron from the HOMO 2e′ or 2e″ in the $^2E'$ or $^2E''$ states of the neutral Al_3P_2 cluster. This yields four states, viz., $^1A_1'$, $^3A_2'$, $^3A_2''$, and $^1A_2'$ for the $Al_3P_2^+$ ion. The energy needed to remove an electron from the open-shell 2e′ HOMO in $^2E'(D_{3h})$ is 6.85 eV, resulting in three possible electronic states with the same configuration: a $^3A_2'$ state, a $^1E'$ state, and a $^1A_1'$ state, among which the $^3A_2'$ state becomes the lowest in energy. Thus, the positive ion does not undergo Jahn−Teller distortion and retains its ideal D_{3h} structure. At the CASSCF level, the lowest state of $Al_3P_2^+$ is $^1A_1'$, while $^3A_2'$ is only 0.04 eV above $^1A_1'$. However, this energy separation is sensitive to higher-order

TABLE 2: Geometries and Energy Separations of Al_3P_2, Al_2P_3 with tbp-D_{3h} Structures[a]

	state		CASSCF				MRSDCI			
system	C_{2v}	D_{3h}	Al−Al (Å)	Al−P (Å)	P−P (Å)	E (eV)	Al−Al (Å)	Al−P (Å)	P−P (Å)	E (eV)[a]
Al_3P_2	$^2A_1$, $^2B_2$	$^2E'$	3.619	2.439	2.516	0.33	3.608	2.430	2.503	0.23 (0.20)
	$^2B_1$, $^2A_2$	$^2E''$	4.032	2.585	2.248	0.65	4.007	2.568	2.229	0.64 (0.54)
	$^4B_1$	$^4A_2''$	2.963	2.483	3.599	2.47	2.907	2.451	3.572	2.11 (1.94)
	$^4A_2$	$^4A_1'$	3.961	2.549	2.252	2.97	3.929	2.532	2.250	2.44 (2.47)
	$^4A_1$, $^4B_2$	$^4E'$	3.412	2.499	3.075	2.73	3.398	2.489	3.064	2.58 (2.38)
	$Al_3(^2A_1) + 2P(^4S)$					6.32				6.77 (7.04)
	$3Al(^2P) + 2P(^4S)$					9.02				10.09 (10.62)
$Al_3P_2^+$	$^3B_2$	$^3A_2'$	3.608	2.430	2.503	6.58	3.608	2.430	2.503	6.85 (6.86)
	$^1A_1$	$^1A_1'$	3.608	2.430	2.503	6.54	3.608	2.430	2.503	7.07 (7.26)
	$^3B_1$	$^3A_2''$	3.608	2.430	2.503	8.43	3.608	2.430	2.503	8.37 (8.33)
	$^1B_1$	$^1A_2''$	3.608	2.430	2.503	9.01	3.608	2.430	2.503	8.91 (8.85)
$Al_3P_2^-$	$^1A_1$	$^1A_1'$	3.737	2.474	2.420	2.14	3.707	2.454	2.400	−2.33 (−2.42)
			P−P (Å)	P−Al (Å)	Al−Al (Å)	E (eV)	P−P (Å)	P−Al (Å)	Al−Al (Å)	E (eV)[a]
Al_2P_3	$^2B_1$	$^2A_2''$	2.300	2.434	4.080	0.00	2.304	2.431	4.070	0.00 (0.00)
	$^2A_2$, $^2B_1$	$^2E''$	2.218	2.700	4.754	0.65	2.209	2.672	4.697	0.76 (0.95)
	$^2A_1$	$^2A_1'$	2.274	2.447	4.130	2.09	2.272	2.431	4.093	1.94 (1.91)
	$^2A_1$, $^2B_2$	$^2E'$	2.274	2.653	4.610	2.11	2.257	2.632	4.573	2.18 (2.25)
	$P_3(^2A_2) + 2Al(^2P)$					7.74				7.90 (7.38)
	$3P(^4S) + 2Al(^2P)$					14.01				14.17 (13.85)
$Al_2P_3^+$	$^1A_1$	$^1A_1'$	2.304	2.431	4.070	6.16	2.304	2.431	4.070	6.79 (6.96)
	$^3B_1$	$^3A_2''$	2.304	2.431	4.070	6.86	2.304	2.431	4.070	7.67 (7.98)
	$^3B_2$	$^3E'$	2.304	2.431	4.070	8.01	2.304	2.431	4.070	8.24 (8.25)
	$^1B_1$	$^1A_2''$	2.304	2.431	4.070	8.87	2.304	2.431	4.070	9.15 (9.19)
$Al_2P_3^-$	$^1A_1$	$^1A_1'$	2.263	2.523	4.317	−2.10	2.250	2.518	4.313	−2.30 (−2.03)

[a] The values in the parentheses are the Davidson corrected energies.

TABLE 3: Vibrational Frequencies and IR Intensities of the Ground States of Al_2P_3, Al_3P_2, and Their Ions

species	vibrational mode, frequency, and IR intensity in parentheses
Al_2P_3[a]	A_1': 481.5 (0), E': 378.8 (1.05), A_1': 338.5 (0), A_2'': 308.6 (15.3), E'': 303.1 (0), E': 175.2 (5.6)
Al_3P_2[a]	A_1: 446.8 (5.0), A_1: 345.2 (15.9), B_1: 338.4 (4.4), A_1: 257.6 (1.0), B_1: 212.5 (13.2), A_2: 192.2 (0), B_2: 159.1 (0.42), A_1: 93.8 (0.4), B_2: 66.2 (22.1)
$Al_2P_3^+$[a]	A_1': 478.0 (0), E': 367.9 (3.7), A_2'': 352.6 (4.0), E'': 345.8 (0), A_1': 328.5 (0), E': 195.4 (11.4)
$Al_3P_2^+$[a]	A_1': 397.2 (0), E': 319.5 (5.5), A_2'': 295.7 (24.4), A_1': 262.8 (0), E'': 237.0 (0), E': 26.7(3.6)
$Al_2P_3^-$[a]	A_1': 504.1 (0), E': 393.8 (0.1), A_2'': 366.8 (83.5), A_1': 303.6 (0), E'': 245.0 (0), E': 146.0 (0.8)
$Al_3P_2^-$[a]	A_1': 410.8 (0), E': 367.8 (0.1), A_1': 268.4 (0), A_2'': 240.9 (7.2), E'': 217.1 (0), E': 115.6 (2.0)

[a] Zero-point corrections for $Al_2P_3 = 5.3$, $Al_3P_2 = 3.0$, $Al_3P_2^+ = 3.0$, $Al_2P_3^+ = 4.2$, $Al_2P_3^- = 3.9$, and $Al_3P_2^- = 3.3$ kcal/mol.

electron correlation effects which stabilize the $^3A_2'$ state, and it prevails as the ground state of $Al_3P_2^+$ at the highest level with the $^1A_1'$ state 0.22 eV above the $^3A_2'$ state at the MRSDCI level. It would need more energy (>1.94 eV) to remove an 1e″ electron from $^2E'$ forming $^3A_2''$ and $^1A_2''$ states, but these are well above the $^3A_2'$ state.

As seen in Table 2, a closed-shell $^1A_1'$ is the ground state of $Al_3P_2^-$ with a regular trigonal bipyramid (D_{3h}) geometry, and the electron affinity of Al_3P_2 is 2.33 eV at the MRSDCI level. The comparison of geometries of the neutral and anion reveals that both Al−Al(3.707 Å) and Al−P(2.454 Å) bonds in the $^1A_1'$ state of $Al_3P_2^-$ become longer, whereas the P−P(2.400 Å) bond length is contracted compared to the corresponding Al−Al (3.608 Å), Al−P(2.430 Å), and P−P(2.503 Å) bond lengths in the $^2E'$ state of Al_3P_2. This suggests that the attached electron is mainly shared by the P atoms resulting in stronger P−P bonds in the $^1A_1'$ state of $Al_3P_2^-$. The attached electron occupies the 2e′ orbital, which becomes fully occupied in $Al_3P_2^-$. Since the P(p_y), P(p_z), and Al(s) are influential components for the 2e′ orbital, the Mulliken populations for $^1A_1'$ of $Al_3P_2^-$ are Al ($s^{1.741}p^{1.057}$), P ($s^{1.811}p^{3.696}$); both P (p) and Al (s) populations are larger than Al ($s^{1.625}p^{0.919}$) and P ($s^{1.807}p^{3.569}$) in the $^2E'$ state of Al_3P_2.

The atomization energy was computed in two steps. The dissociation energy for

$$Al_3P_2 \rightarrow Al_3(^2A_1) + 2\,P(^4S)$$

is computed as 6.77 eV at the MRSDCI level. We also computed the atomization energy needed to separate Al_3 into three Al atoms (^2P) as 3.32 eV at the same level. By combining the two values, the atomization energy of Al_3P_2 is computed as 10.09 eV at the MRSDCI level. These values support our conclusion that the Al−P bonds play a more decisive role than the Al−Al bonds for the energy and geometry of the electronic states of Al_3P_2.

C. Comparison with the Observed Spectra of $Al_3P_2^-$. The only available spectra of Al_3P_2 are due to the work of Gomez et al.[1] The authors have obtained the photoelectron spectra of $Al_3P_2^-$ at 266 nm. In contrast to Al_2P_3, the Al_2P_3 spectra exhibit a less intense and extended progression in the ground state and followed by some activity and a more intense peak around an eV above the ground state. The authors have located the onset of the X peak from which the adiabatic electron affinity of Al_3P_2 is measured as 2.58 eV. As seen from Table 2, our computed adiabatic EA for Al_3P_2 is 2.42 eV at the highest level. We consider this as a very good agreement considering the computational difficulties in computing the EAs of such clusters.

As seen from Table 2, whereas the ground state of $Al_3P_2^-$ is a $^1A_1'$ closed-shell D_{3h} state with a trigonal bipyramidal geometry, the ground state of the neutral Al_3P_2 is a Jahn−Teller distorted $^2A_1$ state arising from the $^2E'$ state of the neutral cluster, which undergoes Jahn−Teller distortion. Thus, the geometries of the neutral and anionic species differ: the latter exhibits a more symmetric structure, while the former undergoes Jahn−Teller distortion to a less symmetric structure. The geometry

differences between the two ground states cause a slightly extended vibrational progression in the X peak of Al_3P_2. A comparison of the actual bond distances of the anion with neutral distorted geometry ($^2A_1$ state) reveals that the axial P−P distances are nearly the same. The contrast is in the Al−Al equatorial distances and thus the Al−P distances: the Al_1-Al_2 distance becomes shorter than the anion, while the Al_2-Al_3 distance becomes longer. Thus the progression in the X state of the observed spectra is due to an equatorial stretch than an axial stretch.

Gomez et al. find ca ouple of short peaks within 0.5−0.75 eV of the X state followed by a prominent peak that is even more intense than the X peak at about 1.3 eV higher than the ground state. As seen from Table 1, we compute the $^2B_1$ Jahn−Teller component of the $^2E''$ state at 0.5−0.6 eV above the ground state, depending on the level of theory. This explains why the observed peaks in this region and the similarly of the intensity of this peak to the ground-state X peak is consistent with our finding in that both the X^2A_1 and A^2B_1 states are Jahn−Teller distorted and thus have similar features in the spectra. In contrast, the next peak is sharp and more intense than the ground state. As seem from Table 2, we compute the $^4A_2'$ excited state of Al_3P_2 at 1.94 eV above the ground state. This state cannot undergo Jahn−Teller distortion and could thus explain the intensity of the observed peak as this state has the same symmetry as the anion's ground state. However, the P−P axial bond is considerably stretched relative to the anion, and the Al−Al equatorial bond distances are contracted. We, however, do not find any other excited state in this region to assign the spectra. Our computations could also have greater errors for the excited states. Thus, the most probable candidate for the observed a peak near 1.3 eV above the ground state is the $^4A_2'$ excited state of Al_3P_2.

D. Nature of Bonding. We describe the composition of the various molecular orbitals (MOs). The $1a_1'$ (or $1a_1$ in C_{2v}) orbital is a bonding combination of $P_1(s) + P_2(s)$. The $2a_1'$ ($3a_1$ in C_{2v}) orbital is composed of $Al_1(s) + Al_2(s) + Al_3(s)$. The $3a_1'$ ($4a_1$ in C_{2v}) orbital is a combination of $P_1(p_x) - P_2(p_x)$ and $P_1(s) + P_2(s)$. The $1a_2''$ ($1b_1$ in C_{2v}) orbital is an antibonding orbital which is composed of $P_1(s) - P_2(s)$. The $2a_2''$ ($3b_1$ in C_{2v}) orbital is predominantly $P_1(p_x) + P_2(p_x)$. The two degenerate components of the $1e'$ ($2a_1$ and $1b_2$ in C_{2v}) orbital are $2Al_1(s) - [Al_2(s) + Al_3(s)]$ and $Al_2(s) - Al_3(s)$. Likewise, the two components of the $2e'$ ($5a_1$ and $2b_2$ in C_{2v}) orbital are composed of $2Al_1(s) - [Al_2(s) + Al_3(s)] + [P_1(p_y) + P_2(p_y)]$ and $[Al_2(s) - Al_3(s)] - [P_1(p_z) + P_2(p_z)]$. The two parts of the $1e''$ orbital ($2b_1$ and $1a_2$ in C_{2v}) are $P_1(p_y) - P_2(p_y) + Al_1(p_x) - [Al_2(p_x) + Al_3(p_x)]$ and $P_1(p_z) - P_2(p_z) + [Al_2(p_x) - Al_3(p_x)]$. The principal difference between the $^2A_1$ and $^2B_1$ (C_{2v}) states is in the occupancies for the $5a_1$ and $2b_1$ orbitals. The $5a_1$ orbital is a combination of two parts: the first part is $2Al_1(s) - [Al_2(s) + Al_3(s)]$ and the second part $[P_1(p_y) + P_2(p_y)]$ is like a Π bonding interaction between two P atoms. The $2b_1$ orbital is a combination of $[P_1(p_y) - P_2(p_y)] + Al_1(p_x) - [Al_2\ (p_x) + Al_3(p_x)]$, suggesting bonding interactions between the Al_1 and P atoms together. The $5a_1$ orbital is singly occupied in $^2A_1$ but fully occupied by $^2B_1$, while the $2b_1$ orbital is fully occupied in $^2B_1$ but singly occupied in $^2A_1$. The $^2A_1$ state has a doubly occupied $2b_1$ orbital, resulting in a shorter Al_1-P bond length (2.279 Å) and longer P−P bond length (2.443 Å) compared to the corresponding values in the $^2B_1$ state. The $P_1-Al_1-P_2$ and $P_1-Al_2-P_2$ angles in $^2A_1$ are 64.8° and 57.3°, respectively. These bond angles are considerably larger than the corresponding values of 48.0° and 50.7°for $^2B_1$, implying that the P−P bonding in $^2B_1$ is stronger than that in $^2A_1$. This is consistent with the P−P bond length in the $^2B_1$ state of 2.178 Å, caused by a doubly occupied $5a_1$ orbital in $^2B_1$.

The main distinction between the $^2E'$ and $^2E''$ states of Al_3P_2 (with D_{3h} symmetry) is in the electron occupations for $2e'$ and $1e''$. As described earlier, the $1e''$ ($2b_1$ and $1a_2$ in C_{2v}) orbital is composed of Al−P bonding, while the $2e'$ orbital contains antibonding interactions among the three Al atoms and a P−P bonding. The $1e''$ orbital is fully occupied by $^2E'$ (four electrons), resulting in a contracted Al−P bond length (2.430 Å) and a longer P−P bond length (2.503 Å), while the $2e'$ orbital is fully occupied in $^2E''$ (four electrons), leading to a short P−P bond length (2.229 Å) and longer Al−P bond length (2.568 Å) at the MRSDCI level. The $2a_2''$ orbital is perpendicular to the Al_3 plane with the p orbitals of the P atoms overlapping with opposite lobes along the *x*-axis. Thus, there exists a repulsive interaction with respect to the P atoms. The $^2E'$ and $^2E''$ states do not have an occupied $2a_2''$ orbital. The $^4A_2''$ state has a doubly occupied $2a_2''$ orbital, while $^4E'$ has a half-filled $2a_2''$ orbital, thus resulting in noticeably longer P−P bond lengths (3.572 and 3.064 Å) in the $^4A_2''$ and $^4E'$ states, respectively, at the MRSDCI level. These features explain the higher energies of all quartet states (D_{3h})of Al_3P_2.

The total Mulliken populations of Al are substantially smaller than 3.0, whereas the total P populations are uniformly larger than 5.0 for all of the electronic states of Al_3P_2. The depletion of the Al population compared to an isolated Al atom and enhancement of the P population compared to the P atom are consequences of charger transfer from the aluminum atoms to the P atoms leading to ionic $Al^+ P^-$ bonding in the Al_3P_2 cluster.

The lowest $^2A_1(C_{2v})$ state of Al_3P_2 is composed of Al_1 ($s^{1.204}p^{1.228}$), Al_2 ($s^{1.817}p^{0.749}$), and P ($s^{1.814}p^{3.601}$) Mulliken populations, where we have omitted the d populations as they are smaller than 0.17. The corresponding populations for the $^2B_1(C_{2v})$ state are Al_1 ($s^{1.859}p^{0.635}$), Al_2 ($s^{1.841}p^{0.735}$), and P ($s^{1.847}p^{3.554}$). The difference between the two states in the C_{2v} symmetry mostly rests with the s and p populations of the Al_1 atom. As discussed before, the primary difference between the two states lies in the occupations and compositions of the $5a_1$ and $2b_1$ orbitals. The $5a_1$ orbital, which has considerable $Al_1(s)$ character, is fully occupied in the $^2B_1$ state, resulting in a large $Al_1(s)$ population of 1.859. The $5a_1$ orbital is singly occupied in $^2A_1$, leading to a smaller $Al_1(s)$ population of 1.204 in the $^2A_1$ state. On the other hand, the $2b_1$ orbital, which contains $Al_1(p_x)$ together with $P_1(p_y)$ and $P_2(p_y)$ contributions, is doubly occupied in $^2A_1$ but singly occupied in $^2B_1$. Consequently, this increases the *p* populations on Al_1 to 1.228, whereas the $^2B_1$ state has a singly occupied $2b_1$ orbital resulting in smaller Al_1 (p) population of 0.617. Similarly, the nature of the $2e'$ and $1e''$ orbitals and their occupation numbers lead to smaller s (1.625) but larger p (0.919) populations on the Al atoms in $^2E'$ (D_{3h}) in comparison with the corresponding populations in $^2E''$ (D_{3h}). As seen in Table 1, the dipole moment of $^2A_1$ (C_{2v}) is 2.69 D, which is larger in magnitude than 1.34 D for $^2B_1$.

A critical comparison of the Mulliken populations of the neutral cluster and the positive ion reveals that the ionization particularly causes depletion of the charge density on the 3s and 3p orbitals of Al rather than the P site. It agrees with the fact that the ionization potential of Al is lower than that of P.

The $^3A_2'$ and $^1A_1'$ states have the same configuration, and thus, their Mulliken populations are very close. The $^2E'$ state is composed of Al ($s^{1.625}p^{0.919}$) and P ($s^{1.807}p^{3.569}$), in which both Al (s) and Al (p) are noticeably larger than the corresponding values in the $^3A_2'$ and $^1A_1'$ states. Since the $2e'$ orbital is

predominantly Al(s) + Al(p), removal of a 2e′ electron decreases the Al populations.

E. Electronic States of Al_2P_3. The computed properties of two distorted $^2A_2$ and $^2A_1$ electronic states of Al_2P_3 in C_{2v} symmetry are listed in the second half of Table 1. In contrast to Al_3P_2, Al_2P_3 has $^2A_2''$ (D_{3h}) as its ground state. Though the two distorted states $^2A_2$ and $^2A_1$(C_{2v}) are derived from the $^2E''$ and $^2E'$ (D_{3h}) states, the Jahn−Teller stabilization is smaller than the energy separation between $^2A_2''$ (or $^2A_2'$) and $^2E''$ (or $^2E'$). Thus, $^2A_2''$ (D_{3h}) prevails as the lowest state of Al_2P_3. It can be expected that the Al_2P_3 cluster possesses an ideal D_{3h} symmetry with a trigonal bipyramid equilibrium geometry. The $^2A_2$ (C_{2v}) state is 0.19 eV above $^2A_2''$ at the CSSCF level. The electron correlation effects make this energy separation even larger (0.48 and 0.64 eV at the MRSDCI and MRSDCI + Q levels). The $^2E''$ (D_{3h}) state is 0.65 eV above the $^2A_2''$ ground state, while the $^2A_1'$ and $^2E'$(D_{3h}) states are much higher in energy, as both states are about 2.0 eV above the $^2A_2''$ state.

The Jahn−Teller effect in Al_2P_3 can be illustrated by a comparison of the geometrical parameters for the $^2A_2$(C_{2v}) and $^2E''$(D_{3h}) states. As seen from tables, three equilateral P−P bonds (2.218 Å) in $^2E''$ (D_{3h}) are changed into two elongated P_1-P_2 and P_1-P_3 bonds (2.315 Å) and a contracted P_2-P_3 bond (2.093 Å) in $^2A_2$(C_{2v}) by the Jahn−Teller distortion. However, the average P−P bond length in the $^2A_2$(C_{2v}) state is 2.241 Å, which is very close to the P−P bonds in $^2E''$. The Al−Al bond length in the $^2E''$(D_{3h}) state is 4.754 Å which is nearly the same as the average Al−Al distance (4.736 Å) in the $^2A_2$(C_{2v}) state, implying little contribution to the Jahn−Teller distortion from the two Al atoms. Thus, the Jahn−Teller effect moves the three P atoms from their ideal equilateral triangular locations in the distorted states (C_{2v}) of Al_2P_3.

F. Electronic States of $Al_2P_3^+$, $Al_2P_3^-$, Ionization Energy, Electron Affinity and Binding Energies. Table 2 displays the energy separations for four electronic states of $Al_2P_3^+$. The calculated energy to remove a $2a_2''$ HOMO electron from $^2A_2''$(D_{3h}) of the neutral Al_2P_3 cluster is 6.79 eV, resulting in a $^1A_1'$ state as a result of the ionization process. Greater energy would be needed to remove an electron from the $3a_1'$ orbital of the $^2A_2''$ ground state of Al_2P_3, resulting in two excited electronic states, namely, $^3A_2''$ and $^1A_2''$. Their ionization energies are 7.67 and 9.15 eV, respectively. The calculated energy to remove an 1e″ electron from the $^2A_2''$ ground state of the neutral Al_2P_3 is 8.24 eV, resulting in the $^3E'$ state. Among these states, the lowest state is the $^1A_1'$ state, while the $^3A_2''$ state is 0.88 eV above at the MRSDCI level. We thus conclude that the $Al_2P_3^+$ ion would have a closed-shell $^1A_1'$ ground state and it cannot undergo Jahn−Teller distortion.

The ground state of the $Al_2P_3^-$ anion is $^1A_1'$ with a regular trigonal bipyramid D_{3h} structure. Table 2 shows the geometrical parameters. As seen from the table, the electron affinity of Al_2P_3 is 2.30 eV at the MRSDCI level. The P−P (2.250 Å) bond length in the $^1A_1'$ state of $Al_2P_3^-$ is contracted, while the Al−Al (4.313 Å), Al−P (2.518 Å) bond lengths are elongated compared to the corresponding bond lengths of Al−Al (4.070 Å), Al−P (2.431 Å), and P−P (2.304 Å) in the neutral ground state $^2A_2''$. It can be concluded that the attached electron in the anion is shared among three P atoms in $^1A_1'$ of $Al_2P_3^-$. This is consistent with the fact that P has greater EA than Al. However, it should be noted that the calculated EA of Al_2P_3 is smaller than that of Al_3P_2 which is 2.33 eV. Thus, the theoretical value is underestimated. It is estimated that the actual EA of Al_2P_3 should be more than 2.4 eV, and our result is a lower bound. The attached electron in the anion of $Al_2P_3^-$ leads to a doubly occupied $2a_2''$ orbital. The $^1A_1'$ state of $Al_2P_3^-$ is composed of P ($s^{1.835}p^{3.361}$) and Al ($s^{1.744}$ $pp^{1.059}$) Mulliken populations. The corresponding populations for the $^2A_2''$ state of the neutral Al_2P_3 are P ($s^{1.845}p^{3.232}$) and Al ($s^{1.510}p^{0.964}$). Hence, both s and p populations on the Al site in the $^1A_1'$ state are enhanced by the attached electron. This agrees with the nature of the $2a_2''$ orbital, which is predominantly Al (s) and Al (p) orbitals.

The dissociation energy for the process

$$Al_2P_3\,(^2A_2'') \rightarrow P_3\,(^2A_2) + 2Al\,(^2P)$$

was computed to be 7.90 eV at MRSDCI level. Combining this with the atomization energy of P_3[48] to yield three P (^4S) atoms which is 6.27 eV, we have obtained the atomization energy of Al_2P_3 as 14.17 eV at the MRSDCI level.

There is significant decrease in the 3s and 3p Mulliken populations on the Al atoms caused by the ionization. The removed electron comes from $2a_2''$, which has Al (s) and Al (p_x) as its principal components. Thus, charge depletion of the Al site appears in the $^1A_1'$ state of $Al_2P_3^+$.

G. Assignment of Observed Spectra of $Al_2P_3^-$. The anion photoelectron spectra of $Al_2P_3^-$ have been obtained at 266 nm by Gomez et al.[1] The observed spectra differ from $Al_3P_2^-$ in having a very sharp and intense X band followed by a weaker set of peaks. As seen from Table 2, our computations are consistent with this contrast in that both the anions and neutral Al_2P_3 have D_{3h} structures due to their $^1A_1'$ and X^2A_2'' ground states, both of which cannot undergo Jahn−Teller distortion. As seen from Table 2, the geometries of the two species are remarkably similar, except that the Al−Al axial distance is shortened upon removal of the electron from the anion and the P−P distances are elongated. Moreover, as seen from Table 3, we find a totally symmetric stretch vibrational mode to have a frequency of 481 cm^{-1} for the X ground state. This is in close agreement with the observed vibrational progression with a frequency of 465 cm^{-1}. Furthermore, the ground state of Al_2P_3 cannot undergo Jahn−Teller distortion, and we thus assign this to the totally symmetric (A_1') breathing mode of Al_2P_3, which is not IR active but Franck−Condon active in the anion detachment spectrum, as it has totally symmetric A_1' representation, as seen from Table 3. The lowering of symmetry was suggested as a possibility by Gomez et al., but we rule out this on the basis of our computations. This is because the neutral cluster in the X^2A_2'' ground-state cannot undergo Jahn−Teller distortion.

We attribute the peaks near 0.6−0.8 eV to the Jahn−Teller distorted $^2A_2$(C_{2v}) state arising from the distortion of the $^2E''$ state. We have calculated this state at about 0.5−0.6 eV above the ground state at higher levels of theory. Above this state, we find only the $^2A_1'$ undistorted state, which is 1.9 eV higher than the ground state, and it is thus an unlikely candidate for the spectra observed by Gomez et al.

Our computed adiabatic EA is 2.3 eV in reasonable agreement with the experimental value of 2.739 eV deduced by Gomez et al. from the observed onset. Again, considering the difficulties in computing EAs, we believe that this is a reasonable agreement.

H. Nature of Bonding in Al_2P_3 and Ions. The $1a_1'$ orbital ($1a_1$ in C_{2v}) is made of $P_1(s) + P_2(s) + P_3(s)$. The $2a_1'$ ($3a_1$ in C_{2v}) orbital is $[P_2(p_z) - P_3(p_z)] + [Al_1(s) + Al_2(s)]$. The $3a_1'$ ($5a_1$ in C_{2v}) orbital is predominantly $[Al_1(s) + Al_2(s)]$ mixed with $[P_1(s) + P_2(s) + P_3(s)] + P_1(p_y) - [P_2(p_y) + P_3(p_y)]$. The $1a_2''$ ($1b_1$ in C_{2v}) orbital is $Al_1(s) - Al_2(s)$. The $2a_2''$ ($3b_1$ in C_{2v}) orbital is a mixture of $Al_1(s) - Al_2(s)$ and $Al_1(p_x) + Al_2(p_x)$, which is an antibonding orbital because the two Al atoms

not only have s orbitals but also p orbitals overlapping with opposite lobes along the *x* axis. The 1e′ orbital ($2a_1$ and $1b_2$ in C_{2v}) possesses two parts: $2P_1(s) - [P_2(s) + P_3(s)]$ and $[P_2(s) - P_3(s)]$. The 2e′ orbital ($4a_1$and $2b_2$ in C_{2v}) is a combination of $[P_2(p_y) + P_3(p_y)] + [P_2(p_z) - P_3(p_z)]$ and $[P_2(p_y) - P_3(p_y)] + [4P_1(p_z) + P_2(p_z) + P_3(p_z)]$. The 1e″ ($2b_1$ and $1a_2$ in C_{2v}) orbital, which is made of $2P_1(p_x) - [P_2(p_x) + P_3(p_x)]$ together with $[P_2(p_x) - P_3(p_x)]$ and the $[Al_1(p_z) - Al_2(p_z)]$, is non-negligible.

The difference between for the first two low-lying $^2A_2''$ and $^2E''$ (D_{3h}) states is in the occupancies of the $2a_2''$ and 1e″ orbitals. The 1e″ orbital is bonding between the Al and P atoms, and it is fully occupied (four electron) in the $^2A_2''$ state, resulting in shorter Al−P bonds (2.431 Å). The $2a_2''$ orbital consists of a repulsive interaction between the two the two Al atoms in which not only s orbitals but also p orbitals of the Al atoms overlap with opposite lobes along the *x* axis. This explains the higher energy of $^2E''$, which has a doubly occupied $2a_2''$. Hence, the $^2E''$ state has a more elongated Al−Al (4.697 Å) bond than that (4.070 Å) of $^2A_2''$, which has only one electron in $2a_2''$.

Likewise, the difference in the properties for the distorted $^2A_2$ and $^2A_1$ states in the C_{2v} symmetry arises as a consequence of the occupancies of the $5a_1$ and $1a_2$ orbitals. The $5a_1$ orbital is bonding not only between the three P atoms but also two Al atoms. However, the $1a_2$ orbital contains a π antibonding between the P_2 and P_3 atoms. Thus, the $5a_1$ orbital exhibits enhanced bonding, and it is fully occupied in the $^2A_2$ (C_{2v}) state, resulting in lower energy than $^2A_1$ (C_{2v}), which has only an electron in $5a_1$. On the contrary, the $1a_2$ orbital is fully occupied by $^2A_1$ (C_{2v}) leading to a longer $P_2 - P_3$ bond (2.232 Å) compared to the P_2-P_3 (2.093 Å) bonds in the $^2A_2$ (C_{2v}) state.

The Mulliken populations suggest Al^+P^- polarity of bonds for all the electronic states of Al_2P_3. It is notable that the P (p) populations are smaller than the corresponding values for Al_3P_2. This is consistent with the fact that the charge transferred from the two Al atoms to P is shared by three P atoms in Al_2P_3, while the charge transferred from the three Al atoms is shared by two P atoms in the case of Al_3P_2. The Mulliken population differences between the first two undistorted $^2A_2''$ and $^2E''$(D_{3h}) states of Al_2P_3 depend on the Al site, consistent with the nature of the $2a_2''$ and 1e″ orbitals. The 1e″ orbital has a nonnegligible Al (p) participation and is fully occupied in $^2A_2''$. This would result in enhanced 3p population on Al (0.964) in $^2A_2''$, which is larger than that (0.672) of $^2E''$. But the $2a_2''$ orbital has Al(s) as its main component, and it is fully occupied by $^2E''$, leading to a higher 3s population on Al (1.854) in $^2E''$ than that (1.510) of $^2A_2''$.

Among the distorted states of Al_2P_3 (C_{2v} symmetry), the populations of Al(s), P_1(s) and P_2(s) for the $^2A_2$ state are 1.859, 1.848, and 1.873, respectively. They are larger than the corresponding values in the $^2A_1$ state (1.314, 1.837, and 1.834). Since the $5a_1$ orbital is composed of Al(s), P_1(s), and P_2(s), it includes the contributions from the 3*s* orbitals of the Al and P atoms, and it is doubly occupied in the $^2A_2$ state but singly occupied in $^2A_1$. It introduces larger s Mulliken populations on the Al and P atoms in the $^2A_2$ state. The $1a_2$ orbital is composed of 3p of the Al atoms, and it is fully occupied in the $^2A_1$ state, resulting in a larger Al(p) population (1.140) in $^2A_1$ than in $^2A_2$ (0.660).

I. Comparison of M_3P_2 (M = Al, Ga, and In). The isovalent Ga_3P_2 and In_3P_2 clusters were previously investigated by the authors,[31,32] and thus, comparison of the electronic states for the M_3P_2 (M = Al, Ga and In) clusters is warranted. Table 4 lists the energy separations and geometries of the distorted states (C_{2v}), while Table 5 shows the corresponding values for the undistorted electronic states (D_{3h}). There are many similarities among the three clusters. For example, all the three species have two closely spaced low-lying electronic states, $^2E'$ and $^2E''$, in the D_{3h} symmetry, and all the quartet states are well above the lowest state. It is expected that $^2E'$ and $^2E''$ (D_{3h}) would undergo the Jahn−Teller distortion. Consequently, the $^2A_1$ and $^2B_1$ states in C_{2v} symmetry shown in Table 4 are the Jahn−Teller components of the $^2E'$ and $^2E''$ states. Analogous to Al_3P_2, the Ga_3P_2 and In_3P_2 clusters undergo the Jahn−Teller effect, as demonstrated by comparing the geometries of the distorted and undistorted states. As shown in the tables, the averaged M−M bond lengths of the ground states (C_{2v}) for Ga_3P_2 and In_3P_2 are 3.714 and 4.351 Å, respectively. These are comparable to the bond lengths between the three metal atoms that form an equilateral triangular base in the corresponding undistorted states of M_3P_2 (M = Ga, In): 3.665 and 4.450 Å respectively. However, the actual M−M bonds differ. The P−P distances in the ground states (C_{2v}) of M_3P_2 (M = Ga, In) are 2.575 and 2.204 Å, respectively. These values are close to the P−P bond lengths in the undistorted states (D_{3h}): 2.587 and 2.226 Å, respectively, at the same level. The metal bond lengths in the ground states of M_3 are 2.521, 2.51, and 2.97 Å[47−49] for M = Al, Ga, and In, respectively. They are clearly much shorter than the M−M bonds in M_3P_2 shown in Tables 4 and 5. It is concluded that the M−M bonds in M_3P_2 are dramatically weakened by the interaction between M and P.

TABLE 4: Comparison of Geometries and Energy Separations for the Electronic States of M_3P_2 in C_{2v} Structure (M = Al, Ga, In)

system		Al_3P_2		Ga_3P_2		In_3P_2	
state		$^2A_1$	$^2B_1$	$^2A_1$	$^2B_1$	$^2B_1$	$^2A_1$
M_3P_2	$M_2-M_1-M_3$ (deg)	69.5	70.9	67.8	72.8	73.6	67.2
	$P_1-M_1-P_2$ (deg)	64.8	48.0	68.2	49.1	45.2	64.0
	$P_1-M_2-P_2$ (deg)	57.3	50.7	59.3	51.4	47.2	56.7
	M_1-M_2 (Å)	3.529	3.801	3.576	3.812	4.081	3.872
	M_2-M_3 (Å)	4.023	4.409	3.991	4.527	4.890	4.285
	M_1-P_1 (Å)	2.279	2.680	2.296	2.713	2.867	2.467
	M_2-P_1 (Å)	2.547	2.543	2.603	2.599	2.753	2.753
	P_1-P_2 (Å)	2.443	2.178	2.575	2.256	2.204	2.613
	E (CASSCF) (eV)	0.00	0.48	0.07	0.00	0.00	0.64
	E (MRSDCI) (eV)	0.00	0.60	0.00	0.15	0.00	0.21
	E (MRSDCI + Q) (eV)	0.00	0.51	0.02	0.10	0.00	0.16

On the other hand, there exist differences among the three clusters. As seen from Table 4, $^2A_1$ (C_{2v}) is relatively stable ground state of Al_3P_2, while $^2B_1$ is definitely the lowest state for In_3P_2 at all levels of theory. For Ga_3P_2, the lowest state is $^2B_1$ at the CASSCF level. However, it is noticed that the energy separation between the $^2B_1$ and $^2A_1$ states is only 0.07 eV at the CASSCF level and it is sensitive to the electron correlation effects, which influence the ordering of these two states. Finally the $^2A_1$ state becomes the ground state of Ga_3P_2 at the MRSDCI and MRSDCI + Q levels.

The P−P bond lengths of the $^2A_1$ (C_{2v}) ground states in Al_3P_2 and Ga_3P_2 are 2.443 and 2.575 Å, respectively, and both of them are longer than the P−P bond length (2.204 Å) in the $^2B_1$ (C_{2v}) state of In_3P_2, implying a stronger P−P bonding in In_3P_2. This can be understood as indium is more metallic than gallium and aluminum. Since the P−P bond is shorter in In_3P_2, the $P_1-In_1-P_2$ and $P_1-In_2-P_2$ angles in the ground state of In_3P_2 are 45.2 and 47.2°, respectively, compared to the corresponding angles of 64.8° and 57.3° of In_3P_2 and 68.2° and 59.3° of Ga_3P_2, respectively.

All $^2A_1$ states of M_3P_2 have enhanced M_1 (p) populations, while all $^2B_1$ states exhibit larger M_1 (s) populations. This is a

TABLE 5: Comparison of Geometries and Energy Separations for the Electronic States of M_3P_2 in the D_{3h} Trigonal Bipyramid Structure (M = Al, Ga, in)

system	state		CASSCF				MRSDCI			
	C_{2v}	D_{3h}	M−M (Å)	M−P (Å)	P−P (Å)	E (eV)	M−M (Å)	M−P (Å)	P−P (Å)	E (eV)
Al_3P_2	$^2A_1$, $^2B_2$	$^2E'$	3.619	2.439	2.516	0.33	3.608	2.430	2.503	0.23
	$^2B_1$, $^2A_2$	$^2E''$	4.032	2.585	2.248	0.65	4.007	2.568	2.229	0.64
	$^4B_1$	$^4A_2''$	2.963	2.483	3.599	2.47	2.907	2.451	3.572	2.11
	$^4A_2$	$^4A_1''$	3.961	2.549	2.252	2.97	3.929	2.532	2.250	2.44
	$^4A_1$, $^4B_2$	$^4E'$	3.412	3.075	3.075	2.73	3.398	2.489	3.064	2.58
Ga_3P_2	$^2B_1$, $^2A_2$	$^2E''$	4.150	2.650	2.264	0.12	4.097	2.620	2.253	0.12
	$^2A_1$, $^2B_2$	$^2E'$	3.665	2.480	2.587	0.45	3.661	2.472	2.564	0.28
	$^4A_2$	$^4A_1''$	3.183	2.450	3.241	1.63	3.188	2.450	3.234	1.05
	$^4B_2$	$^4A_2'$	2.758	2.425	3.658	1.75	2.754	2.416	3.638	1.08
	$^4A_1$	$^4E'$	3.575	2.620	3.228	2.57	3.511	2.577	3.182	2.18
	$^4B_1$	$^4E''$	3.069	2.578	3.745	2.72	3.009	2.527	3.670	2.22
In_3P_2	$^2B_1$, $^2A_2$	$^2E''$	4.450	2.800	2.226	0.15	4.354	2.760	2.279	0.00
	$^2A_1$, $^2B_2$	$^2E'$	4.000	2.650	2.599	0.93	4.000	2.650	2.599	0.40
	$^4A_2$	$^4A_1''$	3.500	2.650	3.429	2.00	3.468	2.624	3.392	1.24
	$^4B_2$	$^4A_2'$	3.089	2.631	3.869	2.17	3.050	2.600	3.826	1.58
	$^4A_1$	$^4E''$	3.901	2.817	3.384	2.76	3.839	2.775	3.339	2.04
	$^4B_1$	$^4E'$	3.414	2.795	3.963	3.15	3.334	2.728	3.866	2.37

TABLE 6: Comparison of Geometries and Energy Separations for the Electronic States of M_2P_3 in the D_{3h} Trigonal Bipyramid Structure (M = Al, Ga, In)

system	state		CASSCF				MRSDCI			
	C_{2v}	D_{3h}	P−P (Å)	M−P (Å)	M−M (Å)	E (eV)	P−P (Å)	M−P (Å)	M−M (Å)	E (eV)
Al_2P_3	$^2B_1$	$^2A_2''$	2.300	2.434	4.080	0.00	2.304	2.431	4.070	0.00
	$^2B_1$, $^2A_2$	$^2E''$	2.218	2.700	4.754	0.65	2.209	2.672	4.697	0.76
	$^2A_1$	$^2A_1'$	2.274	2.447	4.130	2.09	2.272	2.431	4.093	1.94
	$^2A_1$, $^2B_2$	$^2E'$	2.274	2.653	4.610	2.11	2.257	2.632	4.573	2.18
Ga_2P_3	$^2B_1$	$^2A_2''$	2.373	2.479	4.132	0.15	2.315	2.464	4.140	0.05
	$^2B_1$, $^2A_2$	$^2E''$	2.257	2.760	4.866	0.00	2.215	2.725	4.813	0.11
	$^2A_1$, $^2B_2$	$^2E'$	2.310	2.716	4.732	1.80	2.269	2.685	4.687	1.64
In_2P_3	$^2B_1$, $^2A_2$	$^2E''$	2.229	2.921	5.244	0.35	2.218	2.898	5.199	0.25
	$^2B_1$	$^2A_2''$	2.350	2.652	4.557	0.99	2.323	2.639	4.546	0.65
	$^2A_1$, $^2B_2$	$^2E'$	2.290	2.885	5.128	1.99	2.272	2.861	5.085	1.97

consequence of different occupancies for the $5a_1$ and $2b_1$ orbitals in these two states. The $2b_1$ orbital, which contains M (p) as its main component, is doubly occupied by $^2A_1$ but singly by $^2B_1$, resulting in M (p) populations in the $^2A_1$ states of the three clusters. On the contrary, the $5a_1$ orbital is predominantly M (s), and it is fully occupied in $^2B_1$ but singly occupied in $^2A_1$, leading to enhanced M (s) populations in the $^2B_1$ states of the M_3P_2 species.

The Mulliken populations indicate other differences among the three clusters. The gross P populations in the ground states of Al_3P_2 and In_3P_2 are 5.574 and 5.624, respectively, implying that there is more charge transfer from the In to P atoms in In_3P_2. This is consistent with the fact that the indium atom is more electropositive than Al.

J. Comparison of M_2P_3 (M = Al, Ga, and In). There are some striking differences among the three clusters of M_2P_3 compared to M_3P_2. Table 6 displays the geometries and energy separations for the electronic states of M_2P_3 in the D_{3h} trigonal bipyramid structure. As seen from the table, the $^2A_2''$ and $^2E''$ (D_{3h}) states are the first two low-lying electronic states in all three M_2P_3 clusters, and they are comparatively close in energy while the other doublet states ($^2A_1'$ and $^2E'$) are well above the ground state (>1.64 eV). In the case of Al_2P_3, $^2A_2''$ (D_{3h}) is the ground state. But for Ga_2P_3, the $^2E''$ (D_{3h}) state is the lowest state in at the CASSCF level and would undergo the Jahn−Teller distortion. However, the $^2A_2''$ state is 0.15 eV immediately above the $^2E''$ state at the same level and this energy separation is sensitive to the electron correlation effects and thus the energy order of these two states changes. The Jahn−Teller distortion energy is 0.11 eV at the MRSDCI level, and finally, the distorted $^2B_1$ (C_{2v}) state turns out to be the ground state of Ga_2P_3. The undistorted $^2A_2''$ (D_{3h}) is nearly-degenerate with the distorted $^2B_1$ (C_{2v}) because the energy separation between $^2B_1$ and $^2A_2''$ is only 0.05 eV at the MRSDCI level. In the case of the In_2P_3 cluster, the $^2E''$ (D_{3h}) state is 0.64 and 0.40 eV above the $^2A_2''$ state at the CASSCF and MRSDCI levels, respectively. It is expected that the $^2E''$ (D_{3h}) state would undergo the Jahn−Teller distortion; thus, the distorted $^2B_1$ (C_{2v}) state is naturally the ground state of In_2P_3.

As can be seen from Tables 5 and 6, the M−M bond lengths in the ground state (D_{3h}) of M_2P_3 are even longer compared to the M−M bonds in the ground state (D_{3h}) of M_3P_2, implying that the M−M bonds in M_2P_3 are further weakened in the clusters M_2P_3. It can be concluded that the P−P and P−M bonds play a more important role in M_2P_3 compared to M_3P_2.

Following the periodic trend, the In−In bond length in In_2P_3 is longer than the corresponding Al−Al and Ga−Ga bonds in Al_2P_3 and Ga_2P_3. The P−P bond length (2.229 Å) in the ground state of In_2P_3 is the shortest among the three clusters considered here. The reason can be easily understood by the fact that the In atom is located below the Al and Ga atoms within the same column in the periodic table, and thus In is more metallic than the Al and Ga atoms. With shorter P−P but longer In−In bonds in In_2P_3, the In_1-P-In_2 angle in the ground state of In_2P_3 is 127.7°, and it is more open compared to 113.9° for Al_2P_3 and 112.9° for Ga_2P_3.

We note that the gross In (s) In_2P_3 is 1.901, which is significantly larger than the corresponding value for Al (1.510) in $^2A_2''$ (D_{3h}) and Ga (1.624), respectively. This should be mainly due to the relativistic mass-velocity stabilization[50] of the $5s^2$ shell of the indium atom in comparison to the $3s^2$ and $4s^2$ shells of aluminum and gallium atoms, respectively. This

is also the primary factor for the weakening of the metal−metal bond in the electronic states of In_2P_3 in comparison to that of Al_2P_3 and Ga_2P_3.

The matrix-isolated ESR spectra of Ga_2As_3 in Ar and Kr matrixes were observed by Van Zee et al.[12] Comparing their results with those for the isovalent M_2P_3 is of interest. The matrix ESR of Ga_2As_3 reveals that it is in a doublet spin state. The hyperfine structure consistent with three equivalent As atoms arranged in a regular trigonal bipyramidal structure. As seen from Table 6, the regular $^2A_2''$ (D_{3h}) state prevails as the ground state of Al_2P_3, and it would not undergo the Jahn−Teller distortion. Although the distorted $^2B_1$ state is the lowest state for the Ga_2P_3 cluster at the MRSDCI level, the undistorted $^2A_2''$ (D_{3h}) state is nearly degenerate with the $^2B_1$ state. Therefore, either state can be favored in the matrix, but high-order correlation effects seem to favor the D_{3h} structure. The In_2P_3 cluster definitely has a distorted $^2B_1$ ground state. Thus, we expect some similarity among Ga_2As_3, Al_2P_3 and Ga_2P_3, but In_2P_3 differs from the lighter analogues.

Acknowledgment. The research at UC Davis was supported by US National Science Foundation grant CHE9814056 and the work at LLNL was carried out under the auspices of U.S. DOE under Contract Number W-7405-Eng-48. The authors would like to thank Dr. CunYuan Zhao for his help in vibrational frequency computations.

References and Notes

(1) Gomez, H.; Taylor, T. R.; Neumark, D. M. *J. Phys. Chem. A* **2001**, *105*, 6886.

(2) Taylor, T. R.; Asmis, K. R.; Gomez, H.; Neumark, D. M. Vibrationally Resolved Anion Photoelectron Spectra of GaX_2^-, Ga_2X^-, $Ga_2X_2^-$, and $Ga_2X_3^-$ (X = P, As). *J. Chem. Phys.*, in press.

(3) Taylor, T. R.; Asmis, K. R.; Gomez, H.; Neumark, D. M. *Eur. J. D.* **1999**, *9*, 257. Asmis, K. R.; Taylor, T. R.; Neumark, D. M. *Chem. Phys. Lett.* **1999**, *308*, 347. Taylor, T. R.; Neumark, D. M. Private communication, 1999.

(4) Asmis, K. R.; Taylor, T. R.; Neumark, D. M. *J. Chem. Phys.* **1999**, *111*, 8838. Asmis, K. R.; Taylor, T. R.; Neumark, D. M. *J. Chem. Phys.* **1999**, *111*, 10491;

(5) Arnold, C. C.; Neumark, D. M. *J. Chem. Phys*. **1994**, *99*, 3353. Arnold, C. C.; Neumark, D. M. *J. Chem. Phys*. **1994**, *100*, 1797. Arnold, C. C.; Neumark, D. M. *Can. J. Phys*. **1994**, *72*, 1322.

(6) Xu, C.; deBeer, E.; Arnold, D. W.; Neumark, D. M. *J. Chem. Phys*. **1994**, *101*, 5406.

(7) Burton, G. R.; Xu, C.; Arnold, C. C.; Neumark, D. M. *J. Chem. Phys*. **1996**, *104*, 2757.

(8) Bernstein, E. R. Atomic and Molecular Clusters. *Stud. Phys. Theor. Chem.* **1990**, *68*, 69.

(9) O'Brien, S. C.; Liu, Y.; Zhang, Q. L.; Heath, J. R.; Tittel, F. K.; Curl, R. F.; Smalley, R. E. *J. Chem. Phys*. **1986**, *84*, 4074. Liu, Y.; Zhang, Q. L.; Tittel, F. K.; Curl, R. F.; Smalley, R. E. *J. Chem. Phys*. **1986**, *85*, 7434. Wang, L.; Chibante, L. P. F.; Tittel, F. K.; Curl, R. F.; Smalley, R. E. *Chem. Phys. Lett*. **1990**, *172*, 335. Lou, L.; Wang, L.; Chibante, P. F.; Laaksonen, R. T.; Nordlander, P.; Smalley, R. E. *J. Chem. Phys*. **1991**, *94*, 8015. Lou, L.; Nordlander, P.; Smalley, R. E. *J. Chem. Phys.* **1992**. *97*, 1858. Jin, C.; Taylor, K.; Conciecao, J.; Smalley, R. E. *Chem. Phys. Lett*. **1990**, *175*, 17.

(10) Kolenbrander, K. D.; Mandich, M. L. *J. Chem. Phys.* **1990**, *92*, 4759. Rinnen, K.-D.; Kolenbrander, K. D.; DeSantolo, A. M.; Mandich, M. L. *ibid.* **1992**, *96*, 4088. Rasanen, M.; Heimbrook, L. A.; Schwartz, G. P.; Bondybey, V. E. *J. Chem. Phys.* **1986**, *85*, 86.

(11) Li, S.; Van Zee, R. J.; Weltner, W., Jr. *J. Phys. Chem.* **1993**, *97*, 11393. *J. Chem. Phys*. **1994**, *100*, 7079.

(12) Van Zee, R. J.; Li, S.; Weltner, W., Jr. *J. Chem. Phys*. **1993**, *98*, 4335.

(13) Xu, C.; Burton, G. R.; Taylor, T. R.; Neumark, D. M. *J. Chem. Phys* **1997**, *107*, 3428.

(14) Xu, C.; Taylor, T. R.; Burton, G. R.; Neumark, D. M. *J. Chem. Phys* **1998**, *108*, 1395.

(15) Taylor, T. R.; Asmis, K. R.; Xu, C.; Neumark, D. M. *Chem. Phys. Lett.* **1998**, *297*, 133.

(16) Lou, L.; Wang, L.; Chibante, L. P. F.; Laaksonen, R. T.; NordLander, P.; Smalley, R. E. *J. Chem. Phys*. **1991**, *94*, 8015.

(17) Lou, L.; NordLander, P.; Smalley, R. E. *J. Chem. Phys*. **1992**, *97*, 1858.

(18) Wheeler, R. G.; LaiHing, K.; Wilson, W. L.; Duncan, M. A. *J. Chem. Phys*. **1988**, *88*, 2831.

(19) LaiHing, K.; Chen, P. Y.; Duncan, M. A. *J. Phys. Chem.* **1987**, *91*, 6521.

(20) Bishop, M. B.; LaiHing, K.; Cheng, P. Y.; Peshcke, M.; Duncan, M. A. *J. Phys. Chem.* **1989**, *93*, 1566.

(21) Willey, K. F.; LaiHing, K.; Taylor, T. G.; Duncan, M. A. *J. Phys. Chem.* **1993**, *97*, 7435.

(22) Micic, O. I.; Sprague, J. R.; Curtis, C. J.; Jones, K. M.; Machol, J. L.; Nozik, A. J.; Giessen, B.; Flugel, B.; Mohs, G.; Peyghambarian, N. *J. Phys. Chem*. **1995**, 99, 7754.

(23) MacDougall, J. E.; Eckert, H.; Stucky, G. D.; Herron, N.; Wang, Y.; Moller, K.; Bein, T.; Cox, D. *J. Am. Chem. Soc*. **1989**, *111*, 8006.

(24) Andreoni, W. *Phys. Rev. B* **1992**, *45*, 4203.

(25) Balasubramanian, K. *Chem. Phys. Lett*. **1988**, *159*, 71.

(26) Balasubramanian, K. *Chem. Rev.* **1990**, *90*, 93.

(27) Balasubramanian, K. *Chem. Rev.* **1989**, *89*, 1801.

(28) Meier, U.; Peyerimhoff, S. D.; Grien, F. *Chem. Phys.* **1991**, *150*, 331.

(29) Liao, M. Z.; Dai, D.; Balasubramanian, K. *Chem. Phys. Lett*. **1995**, *239*, 124.

(30) Feng P. Y.; Balasubramanian, K. *Chem. Phys. Lett.* **1997**, *265*, 547.

(31) Feng P.Y.; Balasubramanian, K. *Chem. Phys. Lett*. **1998**, *283*, 167.

(32) Al-Laham, M. A.; Trucks, G. W.; Raghavachari, K. *J. Chem. Phys*. **1992**, *96*, 1137. Al-Laham, M. A.; Raghavachari, K. *J. Chem. Phys.* **1993**, *98*, 8770. *Chem. Phys. Lett.* **1991**, *187*, 13.

(33) Archibong, E. F.; Gregorious, R. M.; Alexander, S. A. *Chem. Phys. Lett.* **2000**, *321*, 523.

(34) Tomasulo, A.; Ramakrishna, M. V. *J. Chem. Phys.* **1996**, *105*, 10449.

(35) Korambath, P. P.; Karna, S. P. *J. Phys. Chem. A.* **2000**, *104*, 4801. Korambath, P. P.; Singaraju, B. K.; Karna, S. P. *Int. J. Quantum Chem.* **2000**, *77*, 563.

(36) Arratia-Perez, R.; Hernandez-Acevedo, L. *J. Chem. Phys.* **1998**, *109*, 3497. Arratia-Perez, R.; Hernandez-Acevedo, L. *J. Chem. Phys.* **1999**, *110*, 10882.

(37) Dutta, A.; Chattopadhyay, A.; Das, K. *J. Phys. Chem. A* **2000**, *104*, 9777. Manna, B.; Das, K. *J. Phys. Chem. A* **1998**, *102*, 9876.

(38) Feng, P. Y.; Balasubramanian, K. *Chem. Phys. Lett.* **1999**, *301*, 458. Feng, P. Y.; Balasubramanian, K. *J. Phys. Chem. A* **1999**, *103*, 9093. Feng, P. Y.; Balasubramanian, K. *Chem. Phys. Lett.* **2000**, *318*, 417.

(39) Feng, P. Y.; Dai, D.; Balasubramanian, K. *J. Phys. Chem. A* 2000, **104**, 422.

(40) Balasubramanian, K. *J. Phys. Chem. A* **2000**, *104*, 1969.

(41) Pacios, L. F.; Christiansen, P. A. *J. Chem. Phys.* **1985**. *82*, 2664. Hurely, M. M.; Pacios, L. F.; Christiansen, P. A.; Ross, R. B.; Ermler, W. C. *J. Chem. Phys.* **1986**. *84*, 6840.

(42) Schmidt, M. W.; Baldridge, K. K.; Boatz, J. A.; Elbert, S. T.; Gorden, M. S.; Jensen, J. H.; Koseki, S.; Matsunaga, N.; Nguyen, K. A.; Su, S. J.; Windus, Dupuis, M.; Montgomery, J. A. *J. Comput. Chem*. **1993**, *14*, 1347.

(43) Balasubramanian, K. *Chem. Phys. Lett.* **1986**, *127*, 324.

(44) The major authors of ALHEMY II are Liu, B.; Lengsfield, B.; Yoshimine, M.

(45) Balasubramanian, K. *J. Chem. Phys.* **2000**, *112*, 7425.

(46) Basch, H. *Chem. Phys. Lett.* **1987**, *136*, 289.

(47) Balasubramanian, K.; Sumathi, K.; Dai, D. *J. Chem. Phys.* **1991**, *95*, 3494.

(48) Balasubramanian, K.; Feng, P. Y. *Chem. Phys. Lett.* **1988**, *146*, 155.

(49) Balasubramanian, K. *Relativistic Effects in Chemistry: Part A, Theory and Techniques*; Wiley-Interscience: New York, 1997; p 381. Balasubramanian, K. *Relativistic Effects in Chemistry: Part B, Applications*; Wiley-Interscience: New York, 1997; p 527.

(50) Huber, K. P.; Herzberg, G. Molecular Spectra and Molecular Structure. *Constants of Diatomic Molecules*; Van Nostrand Reinhold: New York, 1979.